International Innovative Research Journal of Engineering and Technology
ISSN: 2456-1983 Vol: 5 Issue: 2 December 2019

Performance of the Connection Budget of a Wireless Communication Network in Ultra Wideband Systems

Emmanuel O.C. Mkpojiogu[1], Zabidin Husin[2]
[1]Department of Computer and Information Technology, Veritas University Abuja, Nigeria
[2]School of Computing, Universiti Utara Malaysia, 06010 UUM Sintok, Kedah, Malaysia

Abstract: An experiment is identified and analyzed to study the multi-path transmission of ultra-wideband (UWB) chaotic microwave array radio pulses through a wireless network within buildings. The limitations imposed on chaotic radio pulses by multipath propagation are defined on the connection margin of UWB communication lines.

Keywords: Wireless Communication, Ultra Wideband Systems, Microwave

I. INTRODUCTION

The design of wireless ultra-wideband (UWB) systems for the transmission of information in the microwave range includes learning the laws of multipath channel propagation and processing UWB signals [1]. The development of new forms of wireless UWB communication channels is continuously followed by the formation of UWB communication channels. The image of multipath propagation, folding in each particular case, depends on a number of unpredictable factors: the relative position of the transmitter and receiver, the geometry and room type (or environment) and the distance between the transmitter and receiver. Research and development of multi-path propagation models therefore begins with the collection of empirical experimental data on the distribution of rays entering the receiver under certain conditions. The products of experimental measurements were numerical models representing multi-path channels based on their average characteristics [1].

Mass-use UWB communication systems were initially conceived as a means of coordinating wireless high-speed communication between multimedia consumer devices [2]. UWB signals were then included in the wireless sensor network standard [3, 4]. In addition, these signals started to be used to coordinate the transmission of wireless data in body networks [5].

During the development of multi-channel models for IEEE 802.15.3a [2] and IEEE 802.15.4a [4, 6–8], the main patterns of propagation of UWB signals for short-range network communication systems were recorded. Such models, however, do not cover the entire range of possible UWB systems implementations that are constantly expanding. Therefore, in new areas of application, it is necessary to go beyond the specified models and identify patterns of propagation of UWB signals.

For example, the conditions for the propagation of UWB signals on a fueling station's territory have been analyzed in [9] where, according to the authors, information terminals can be located for wireless high-speed access to multimedia data while the vehicle is parked. The transmitter-receiver length ranged from 2 to 20 m. At ranges up to 60 m (wood), up to 52 m (village) and up to 70 m (hills) the properties of the UWB canal in the woods were also investigated [10].

UWB communication channels were studied in the range from 3 to 9 GHz when propagating signals indoors at distances of up to several tens of meters [11]. In [12], consideration was given to the question of the adequacy of the description of the propagation of an IEEE 802.15.4a UWB signal model at distances up to 70 m. Interesting is the work [13] where the UWB communication channel is investigated between the operator and unmanned aircraft.

The main type of UWB signal in the above-mentioned literature is ultrashort pulses (USP), with the help of which the attenuation rate of signal power with increasing distance and shading statistics and small-scale channel fading are determined in the course of experimental studies.

There are other types of UWB signals that can be carriers in a wireless channel as well as ultrashort pulses. One is the chaotic pulses of UWB radio [14]. This signal type is included in IEEE standards 802.11.4a [3] and IEEE standards 802.11.6 [5]. Unlike an ultrashort pulse, the bandwidth and duration of chaotic radio pulses may vary with each other independently. This property helps us to solve two problems while transmitting information in a wireless network. First, to generate the pulse energy is possible, regardless of the transmission band, by adjusting its duration [15] and thus making it possible to communicate. Furthermore, the length of such a pulse can be matched to a multi-path channel response time to prevent pulse degradation due to the small-scale fading caused by multiple rays being placed on each other at the receiving point [16].

International Innovative Research Journal of Engineering and Technology
ISSN: 2456-1983 Vol: 5 Issue: 2 December 2019

These two qualities can be used to increase the UWB channel's link margin. The communication line's power reserve for a channel with noise (link margin) [17] is the ratio of the effective signal-to-noise value in terms of a bit of information transmitted at the receiving point to the minimum possible signal-to-noise value also in terms of the bit for which the communication channel provides the necessary likelihood of error per bit. The increase in the link margin is important for any sort of communication line, as it not only increases the formally achievable free space transmission distance, but can also be used to compensate for the unforeseen interference that cannot be foreseen in the widely used wireless communication networks that are wireless sensor networks. In the class of UWB wireless sensor networks designed to transmit multimedia streaming data, this problem is especially acute [18,19].

An increase in the connection margin due to an increase in the length of the accumulation of a chaotic radio pulse in the receiver leads to a reduction in the speed of transmission, which is inacceptable in some situations. Therefore, by increasing the power of the pulses it is necessary to increase the signal-to-noise ratio at the receiving point. This is related to the task of increasing the communication range with respect to the distances (up to 30 m) set out in the wireless standard IEEE 802.15.4a low speed [3].

The multi-path pattern, which is detected by a receiver with a finite sensitivity, would reflect an increase in the intensity of chaotic radio pulses. The purpose of the study is therefore to examine how the power increase affects the outcome of multi-path propagation at the receiving point and how this can ultimately affect the selection of other parameters: the pulse service cycle (pulse frequency) and the sensitivity of the receiver. The research was carried out in the wireless channel inside the room based on the experimental measurements of the propagation outcome of the unpredictable UWB radio pulses of the microwave range.

II. LINK MARGIN OF CHANNEL UWB WITH PROPAGATION MULTIPATH

The conventional method used today in UWB channels to describe multipath propagation is the construction of beam models [1]. First of all, multi-path propagation of UWB signals of any type must be simulated. In this paper, on the level of the envelope of chaotic radio pulses, multipath propagation is analyzed. For the following reasons, this is recommended. It is important that information about the amplitude and delay of chaotic radio pulses at the receiving point is irretrievably lost after passing a chaotic radio pulse multipath channel, generating tens and hundreds of rays that are separated in time by several nanoseconds. The current method of studying the multipath stream, which consists of calculating the distribution of the arrival of rays in time and amplitude, in the case of the use of unpredictable radio pulses, is therefore impractical to replicate fully. It makes sense to analyze only the pulse signal envelope as an indicator by which you can determine from the delay time the average power distribution of the incoming rays. As the value characterizing the attenuation of the UWB signal in the propagation medium, it is also important to determine the attenuation of the signal power from the distance between the emitter and the receiver.

Energy profile analysis is relevant not only for chaotic radio pulses [20, 21] but also for ultrashort pulses and ultrashort pulses, as this information enables us to build optimal energy reception schemes in a multi-path channel [22–31].

A generator of chaotic UWB oscillations [32,33] produces the carrier signal in UWB communication systems on chaotic signals by modulating it with video pulses. Chaotic UWB radio pulses T_P (Fig. 1a) are generated at the generator output, which can vary from 10 to 1000 ns in the existing equipment [14,18,19], which is sufficient to cover the entire range of multipath echo. A passive interval of duration follows the impulse. T_G to prevent interference with interpulses. The pulse position together with the guard interval position forms the symbol duration position $T_S = T_P + T_G$. Duty Pulse Area $D = (T_P + T_G)/T_P$.

Let P_s be the power of a chaotic signal and it occupies band W until $f_2 = f_1 + W$ on frequency f_1. By definition [17], the link margin of a noise channel communication line is the ratio E_B / N_0 to the minimum acceptable value $(E_B / N_0)_0$ at the reception point, for which the communication line provides the required probability of error per bit.

$M_N = (E_B/N_0) / (E_B/N_0)_0 = (P_S/P_N) / (P_S^{(0)}/P_N)$ (1)

Where $(E_B / N_0) = (P_S / P_N) (W / R_B)$, $P_S^{(0)}$ is the minimum signal power entering a direct beam with the necessary error level per bit, R_B is the transmission speed (bit/s) directly proportional to the pulse transmission frequency and N_0 is the density of spectral noise. The relationship W / R_B is the gain for a direct coupling system, depending on the length of the pulse: $W / R_B = WT_S = WT_P / D$.

Multipath propagation becomes an obstacle when interpulse interference occurs, resulting from the introduction of rays by energy due to the short duration of their accuracy (Fig. 1b), outside the pulse nominal position. This can lead to pulse reception errors if the guard interval duration is less than the delay in the propagation of the reflected rays. Thus, the combination of impulses 10 at 0 can result in an error occurring.

International Innovative Research Journal of Engineering and Technology
ISSN: 2456-1983 Vol: 5 Issue: 2 December 2019

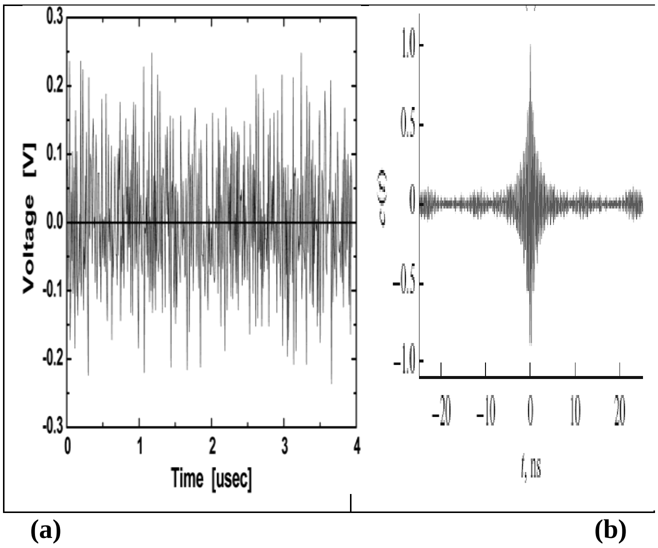

Figure 1. (a) Execution of the chaotic radio pulse and (b) the chaotic signal of autocorrelation function

Here 1 shows the presence of a pulse and 0 shows its absence in a given temporary position. Combinations of a pair of pulses 00, 01 and 11 do not result in errors in the position of the second pulse, provided that the delays in the arrival of the rays are limited to the time interval equal to the total duration of the two following pulse positions. Multipath interference thus plays the role of additional interference with white noise P_M [21], for which the expression for the link margin can be written by analogy with (1).

$$M_M = (P_S/P_M) / (P_S^{(0)}/P_M) = P_S/P_S^{(0)} \quad (2)$$

If PM >> PN is of interest to the multi-path network to examine such an event.

Simultaneously, the frequency of multi-path interference P_M depends on the length of the T_G (or duty ratio) guard interval [16]. The less energy P_M due to the current momentum, the greater the guard interval.

Therefore, we can control the noise immunity of UWB communication circuits in the multi-path channel by using three parameters that define a specific value M_M — the power of chaotic UWB radio pulses P^S, their duration, and duty cycle D.

We will also consider the reference margin of the UWB channel on chaotic radio pulses in the Additive White Gaussian Noise (AWGN) system as a starting point. The limitations on the allowable power spectral density of a chaotic signal actually determine the link margin in the AWGN channel. Below we analyze this reserve's boundaries.

The average spectral power density of the transmitted signal is proportional to the average pulse repetition rate due to the pulsed nature of the carrier signal and the packet data transmission system. Then the unmodulated chaotic signal's spectral power density will be P_S / W. P_S/ (2WD) will be the average power spectral density of the sequence of chaotic radio pulses followed by a duty cycle D equipped with zero and single pulses.

The average power spectral density will be N_S= P_S ($2WDD_P$) since the information is transmitted in a batch manner and the burst ratio is D_P. Thus, ceteris paribus, the freedom of choice of the pulse power appears while maintaining the average spectral power of the radiation by varying the average pulse repetition frequency.

For example, in free space (a channel with additive Gaussian white noise, the signal power decreases inversely to the square of the distance between the transmitter and the receiver), all other conditions being equal, P_S and therefore the contact margin (1) can be increased $2DD_P$ times by increasing the radiation power in the pulse $2DD_P$ times without changing the average spectral radiation intensity. This cost will be ~80 for a work ratio D = 2 and batch duty period D_P = 20.

Under multi-path channel conditions, this means that at the point of reception rays with a path length of about nine times longer than the original are involved in creating a multi-path pattern. The multi-path power P_M will increase with the increasing power of the emitted pulses P_S so that the connection margin (2) changes in the multi-path stream.

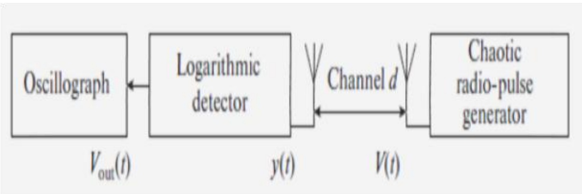

Multipath propagation experiments with chaotic UWB radio pulses with a power between 1 and 100 mW were performed in this study.

An energy receiver with a sensitivity of about 10^{-8} mW was used in the experiment. This sets a maximum of ~10^{10} times (10^2 mW/10^{-8} mW or 100 dB) change in signal power, which formally corresponds to an equivalent shift in signal power with a frequency of 3 GHz in free space at ranges up to 200 m. The distance limit sets the value that can be calculated for the maximum range of rays.

For a pulse power of 1 mW, a factor of ten will minimize the mean free path of the rays set by the receiver in free space; i.e., it will be about 20 m. Therefore, by comparing the result of the propagation of pulses with a power of 1 and 100 mW, the influence of the multi-path channel on the shape of the pulse envelope at the receiving point will be identified and the communication lines resulting from this limitation on the link margin will be formulated.

III. EXPERIMENT OF THE MAP MARGIN IN A CHANNEL MULTIPATH

The experimental measurement scheme is shown in Fig. 2: The chaotic generator generates chaotic radio pulses

International Innovative Research Journal of Engineering and Technology
ISSN: 2456-1983 Vol: 5 Issue: 2 December 2019

passing through a wireless channel and reaching the UWB input of a logarithmic detector forming a signal envelope of chaotic radio pulses at its output. The envelope's instantaneous amplitude is proportional to the input power logarithm. Such a detector creates a pattern of change over time from the moment it starts in the instantaneous pulse input power. The instant power value is formed as the sum of all the rays that enter the receiver. The effect of a multi-path channel on the form of the pulse envelope was measured and the attenuation frequency of the power of chaotic radio pulses with distance was calculated within the context of this measurement scheme.

The PPS-47 transceiver [19] was used for measurements, generating a random series of chaotic radio pulses of T_P = 83 ns duration (see Fig. 1a), in which there was a T_G = 83 ns duration guard period. The receiver used in the experiment, which included a logarithmic detector [34] and a low-noise amplifier, had a dynamic range of 80 dB and, in conjunction with a low-noise amplifier with a gain of 100, had a sensitivity of $3\ 10^{-9}$ mW (–85 dBm W).

The detector's cascade structure explains the logarithmic dependence of the output signal amplitude on the input signal power — the detector contains seven serial amplification stages with saturation, each amplifying the signal by ~10 times the power in the cascade's linear zone. In general, therefore, the signal is amplified from 1 to ~107 times in the range. In this case, the amplitude of the output signal takes values from 0.5 to 2 V proportional to the input power logarithm. The logarithmic detector in the linear operating area converts the 80 dB input power spread to a linear output voltage scale.

$$V(r,t) = \alpha 10 \log P(r,t)/P_0 \qquad (3)$$

Where α is the steepness of the logarithmic detector characteristics (in this case α = 0.021 V / dB [34]); P(r, t) is the signal power entering the transmitter at range r from the receiver; and P_0 is the reference power (in this case P_0 = 1 mW).

Assess the form of the pulse envelope after the channel is passed and assess the attenuation in accordance with the scheme in Fig. 2 during the experiments. A storage oscilloscope was used for each distance r_i between the Chaotic Radio Pulse Emitter and the receiver to record the Chaotic Radio Pulse Envelope Signal with a sampling frequency of 2,5 Gs (the oscilloscope Tektronix DPO 4054 was used) and the oscilloscope input frequency was 500 MHz. Chaotic radio pulses ' signal envelope occupied the frequency range between 0 and ~10 MHz.

A waveform with a duration of ~1000 pulse lengths has been fixed for each distance value r_i. There are different combinations of them in the sequence of pulses, including those where there are no adjacent pulses in at least three positions before and after the single pulse.

$$\langle V(r_i,t)\rangle = \frac{1}{N_i}\sum_{j=1}^{N_i} V_j(r_i,t). \qquad (4)$$

For each value r_i, an average of ~100 pulses was performed in the experiment. Analysis of the average form of single pulses allows the effect of multipath propagation to be determined without the influence of interpulse interference. This average is analogous to the communication channel's average energy profile, which characterizes the power change of the UWB signal entering the receiver, with the increasing delay time in response to a delta pulse [4].

The experiments were conducted in the corridor and in the laboratory room at the Kotelnikov Institute of Radio Engineering and Electronics, Russian Academy of Sciences (IREE RAS). The laboratory room was ~5 m long, ~6 m wide, and ~4 m high. It was split into two floors by a steel overlap and lined with a lot of metal structures (see Fig. 3a). The first floor measurements were done. The emitter and receiver's height to the metal overlap is ~1.5 m. The equipment layout in the measuring process is displayed in Fig. 3b.

The measurements of the corridor were as follows: height of about 4 m, length of about 44 m and width of about 3 m. A steel frame with transverse dimensions of approximately 1 x 1 m was extended at a height of approximately 3 m along a corridor (see Fig. 3c). Many metal doors stood in the corridor along the walls. Also, at the end of the corridor, on the opposite side of the one where the receiver was mounted, was a metal door. Throughout its length, fluorescent lamps with a metal casing are suspended on the ceiling of the corridor at an interval of about 5 m. The configuration of the corridor equipment is shown in Fig. 3d.

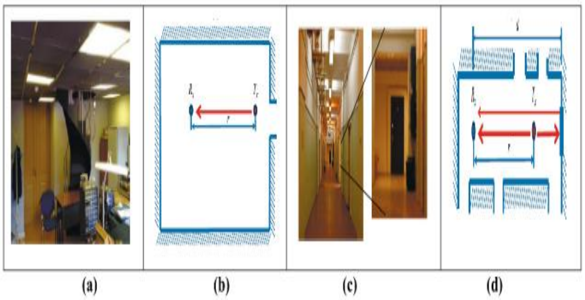

Figure 3. Photographs of measuring site (a, c) and measuring tool design (b, d); R_x is receiver, T_x is radiator. For laboratory (a) 0.5 ≤ r ≤ 4 m; for corridor (c) d = 38 m, 0.5 ≤ r ≤ 32 m, respectively

The range between the emitter and the receiver ranged between 0.5 and 32 m in the corridor and between 0.5 and 4 m in the laboratory: 0.5, 1, 2, and 4 m in the laboratory and 0.5, 1, 2, 4, 8, 16 and 32 m in the corridor were selected. In direct visibility conditions, the emitter and

International Innovative Research Journal of Engineering and Technology
ISSN: 2456-1983 Vol: 5 Issue: 2 December 2019

receiver were located at a height of 1 m from the surface of the floor.

In Figure, an example of an envelope design fragment made in the laboratory for r_1 = 0.5 m is shown. 4. The photo shows a single pulse fragment of the $V_j(r_i, t)$ signal.

Figure 5 shows the average pulse shapes for a pulse corridor of 1 mW (Figure 5a) for ranges between 0.5 and 16 m and between 1 and 32 m: r_1 = 1, r_2 = 2, r_3 = 4, r_4 = 8, r_5 = 16, and r_6 = 32 for pulses of 100 mW (Figure 5b).

Of pulses with a power of 1 mW (Fig. 6a) and 100 mW (Fig. 6b), Figure 6 shows typical pulse shapes for the laboratory. The length r_i ranged between 0.5 and 4 m.

The upper curve corresponds to the minimum distance between the emitter and the receiver in each figure, whereas the lower one corresponds to the maximum distance between the emitter and the receiver.

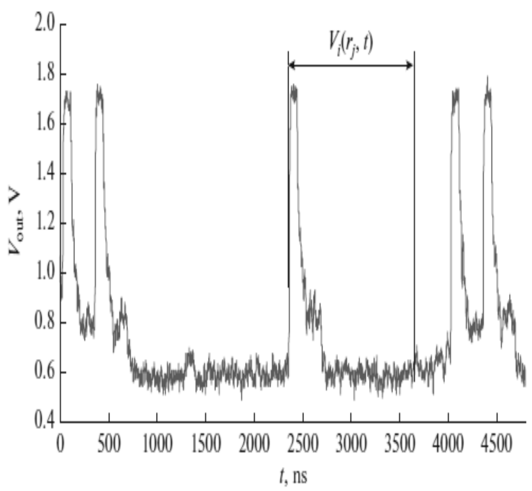

Figure 4. Envelope $V_i(r_j, t)$ pulses at the logarithmic detector output for length r_j and envelope fragment implementation of ith pulse $V_i(r_j, t)$ at the envelope implementation jth

IV. EVALUATION OF VARIABLE RESULTS

In all experiments, the average pulse envelope had a leading edge, rising within 5 ns, and a constant signal amplitude within the measured pulse length.

The preceding signal level had a value of $V_S^{(0)}$ = 0.6V. This is a level of zero equivalent to the lack of a signal at the input of the receiver.

The rate of decline of the trailing edge depends on the conditions of propagation. In the laboratory, from the moment of the nominal end of the pulse, the back front drops more than 70 ns for a 1-mW pulse and it drops more than 120 ns for a 100-mW pulse. This is equal to getting ~21 and ~36 m raids lights.

The response for the corridor stretches to 70 ns for a 1-mW pulse and up to 250 ns for a 100-mW pulse, which in this case is consistent with the typical response period for office-type rooms of the IEEE 802.15.4a [4] multi-path channel model CM5. This is equal to getting ~21 and ~75 m raids lights.

The boundary of the pulse entering directly from the radiator is located in the corridor at the initial part of the pulse signal envelope (Fig. 5b). Therefore, there is a difference between the pulse envelope of a larger amplitude, which reflects the possibility of pulses arriving with some delay due to the presence of a reflector. Depending on the distance between the sender and the receiver, the delay varies. The metal door at the end of the corridor is a candidate for the position of the reflector, which under experimental conditions forms the second beam (see Fig. 3c). This is supported by the analysis of the magnitude of the delay of the delayed beam based on the structure of the distribution of rays in the corridor (see Fig. 3d) and based on the calculation of the delay along the envelope (Fig. 7).

The time marks indicating the falling edge of the $t_{ed}^{(i)}$ ={333, 325, 312, 283, 231, 126 } ns reflected pulses are shown in Fig. 5b. That's right. The difference between moments $\Delta t_{ed}^{(i)}$ and pulse length T_P = 83 ns is equal to the delay time when the pulse arrives due to the twice the difference in the path length of the direct beam from the emitter to the receiver and the distance between the receiver and the door, i.e. 2(d − ri) (see Fig 3d). $\Delta t_{ed}^{(i)}$ = { 250, 242, 229, 200, 148, 43} ns this time difference. The ray incursion reflected 2(d − r_i) in co-ordinates (r_i,2 (d-r_i)) where r_i={ 1, 2, 4, 8, 16, 32} forms a straight line (solid line in Fig. 7). This straight line approximates the calculated raid values (i) c (c is the speed of light) (diamonds in Fig. 7). The difference between the foray measured and the real $|\Delta t_{ed}^{(i)} c - 2(d - r_i)|$ is not greater than 40 cm.

It is possible to determine the law of attenuating the signal energy with the length for a direct beam. The difference between the voltage at the detector output, registered for distance r_1, and the voltage, set for distance r_i proportional to attenuation $P(r_1)/P(r_i)$, is by relationship (3).

$V(r_1) - V(r_i) = 10\alpha$ (log $P(r_1)/P_0 - P(r_i)/P_0) = 10\alpha$ log $P(r_1)/P(r_i)$ (5)

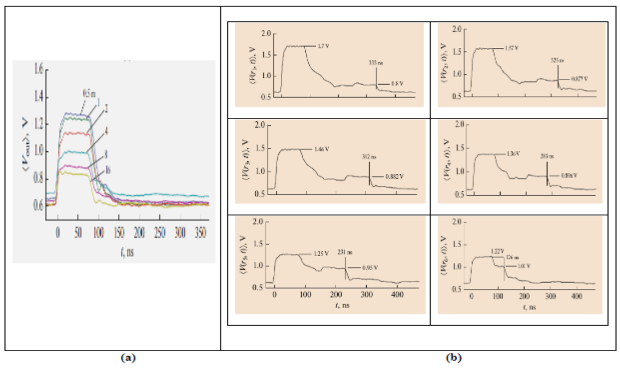

Figure 5. Average form of the pulse envelope for 1 mW (a) and 100 mW (b) pulses in the corridor

MELANGE PUBLICATIONS
International Innovative Research Journal of Engineering and Technology
ISSN: 2456-1983 Vol: 5 Issue: 2 December 2019

The power P(r) which reaches the receiver in free space at distance r from the radiator falls inversely to the distance square, $\sim P_T / r^2$ where P_T is the power of the signal emitted. The power ratio $P(r_1)$ will then be the signal entering the detector at distance r_1 from the radiator to the $P(r_i)$ input to the distance r_i detector.

$$P(r_1)/P(r_{i1}) = (r_i/r_1)^2 \qquad (6)$$

We can expect [4] the signal strength to decrease with increasing distance $\sim r^{-n}$, where n is the attenuation frequency other than 2 for a multi-path propagation medium, based on the previously developed multi-path UWB channel models. At the same rate, n < 2 for direct beam channels and n < 2 for medium beam channels.
We write the power ratio $P(r_1)$ to power $P(r_i)$ in the form by analogy with the case of free space.

$$P(r_1)/P(r_i) = (r_i/r_1)^n \qquad (7)$$

and considering the voltage relationship (5) at the detector output

$$V(r_1) - V(r_i) = \alpha n 10 \log(r_1/r_i) \qquad (8)$$

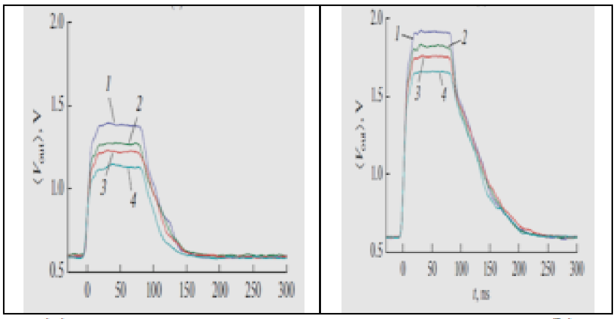

Figure 6. Average shapes of the pulse envelope for 1 mW (a) and 100 mW (b) chaotic radio pulses in the laboratory at different distances between source and receiver r = 0.5 (1), 1 (2), 2 (3) and 4 m (4)

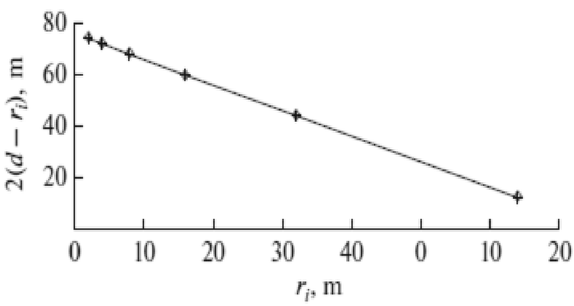

Figue 7. It is relatively straightforward to calculate the size of the raid 2 $(d - r_i)$ of the reflected beam from the path-length direct beam based on measurement geometry (solid line) and measured delays $\Delta t_{ed}^{(i)}$

Thus, by comparing the average amplitude $(V(r_i))$ envelope of chaotic radio pulses for distance r_i with the medium amplitude $(V(r_1))$ pulses for some initial distance r_1, the value of the attenuation index n of UWB chaotic radio pulses can be obtained.

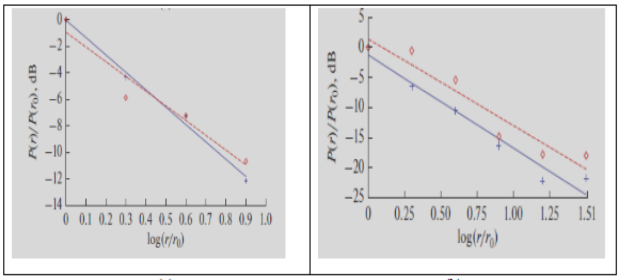

Figure 8. Power ratios $P(r)$ $P(r_0)$ in laboratory (a) and corridor (b) depending on the distance ratio $\log(r/r_0)$. Strong curve is approximation of measurements for pulses of 1-mW (diamonds), the dotted curve is approximation for pulses of 100-mW (crosses)

Figure 8 demonstrates the dependency of the signal energy ratio measured for the distance r_i between the emitter and the receiver at the distance r_1: $P(r_i)$ $P(r_1)$ for the laboratory room (Fig. 8a) and the pulses 1 and 100 mW corridor (Fig. 8b).
The method of approximation of the minimum squares was used to determine the attenuation index n (solid curve) using this data. In lab room n = 1.1 for 1 mW and n = 1.3 for 100 mW; in corridor n = 1.5 for pulses of 1 and 100 mW. The attenuation index is less than two in both forms of hypotheses, suggesting the existence of multipath propagation and demonstrating the effect of multipath amplification [35–37] associated with the incoherent combination of rays.
Multipath amplification increases the free space connection margin of the UWB network. For example, the UWB link margin with the attenuation value n= 1.5 would surpass the free space link margin of the communication channel (n= 2) by 10 log (22−1.5) = 1.5 dB at each doubling of the gap between the emitter and the receiver.
Returning to the measurement results obtained for the corridor (Fig. 5b), we can see that the channel multipath echo lasts ~220 ns after the moment when the nominal pulse location ends (the distance between the transmitter and the receiver r_1 = 1 m). The power of the direct beam signal is ~1.5 $\sim 10^4$ times (~42 dB) higher than the power of the multipath interference (the peak value of the $V_M^{(r1)}$ = 0.8 V reflected beam envelope), which is the reference margin (2): $M_M^{r1} = ((V(r_1)) - V_M(r_1))/\alpha \approx 42$ dB. A single-beam channel reference margin is $M_N = (V(r_1) - V_S^{(0)})/\alpha \approx$ 52 dB.
An increase in distance r between the emitter and the receiver degrades the interference ratio of the signal / multipath and therefore the margin of the connection

International Innovative Research Journal of Engineering and Technology
ISSN: 2456-1983 Vol: 5 Issue: 2 December 2019

decreases. The relation margin (2) for distance r_5 = 16 m is $M_M^{(r5)} \approx 27$ dB. This example shows that this will cause an error if the reflected signal drops to the next pulse position in time. In this case, the error will be related to the incorrect determination of the UWB channel connection margin, determined on the basis of the absence of multipath propagation.

The findings of the laboratory and corridor studies reveal two qualitatively different conditions associated with the transmission of multipaths.

If there are no rays with large delays (measurements in the laboratory (Fig. 6) and in the pulse corridor with a power of 1 mW are shown here), the rays entering the receiver do not result in the pulse enlarging envelope relative to its nominal position, which could result in inter-pulse interference. Due to multi-path interference, there are no restrictions on the communication line's power reserve; therefore, the pulse transmission frequency can not be changed. In this scenario, due to multipath amplification, the contact line's connection margin increases (the attenuation frequency under these conditions is less than two).

If there is a reflector in the channel creating beams with significant delays whose energy at the receiving point exceeds the receiver's sensitivity limit, the power reserve (2) of the communication line will decrease, and this will manifest in the presence of errors when recording pulses in combination 10 at position 0 at which the transmitter did not radiate.

It can be technically implemented in several ways to eliminate the negative effects of rays with large delays as a cause that increases the probability of an error. First, if we consider the presence or absence of a previous impulse and make a decision based on this information during the processing of the current impulse. The design of methods that ensure the blind streaming of the pulse envelope without the need to conduct a preliminary analysis of the communication channel between the transmitter and the receiver to establish the conditions for the propagation of the signal is of interest here. Second, the intensity of the transmitted signal can be reduced. Thirdly, the sensitivity of the receiver can be reduced (in this case by a factor of 100), e.g. by using a managed gain microwave amplifier. The stream is linear; thus, in terms of the result obtained, both of these methods are identical. Comparing the envelope signals for pulses, the propagation of which was determined in the hallway, will explain the last two approaches. The multi-path echo length in the receiver decreases by a factor of ~3.5 when a factor of 100 (by 20 dB) reduces the radiated signal power. If the sensitivity of the receiver is degraded by 20 dB, the same result is achieved. A reduction in the sensitivity of the receiver means that a pulse must be recorded if its envelope exceeds 1 V rather than 0.6 V, which is equivalent to the maximum sensitivity of the receiver (see Figure 5a). The pulse lasts to 140 ns at a rate of 1 V, which is within the pulse nominal location (166 ns) and does not result in interference with the pulse.

V. CONCLUSION

The effect of multipath propagation is evaluated on the UWB contact margin with a chaotic carrier. The experimental limitations associated with multipath propagation that we face when developing methods for receiving UWB pulses and that must be taken into consideration when developing methods for processing the pulse envelope in such receivers.

It is shown that the effect of multi-path propagation is not an insurmountable obstacle in terms of maintaining transmission speed in the sense of UWB pulsed wireless transmission of information under certain conditions and generally plays a positive role as a phenomenon that helps to accumulate a useful signal at the point of reception, raising the communication line's connection margin.

The results obtained on UWB chaotic radio pulses are of practical interest in the design of short-range UWB wireless networks.

REFERENCE

[1] A. F. Molisch, Proc. IEEE 97, 353 (2009).

[2] Channel Modeling Sub-committee Report Final. November 2002. IEEE P802.15 Working Group for Wireless Personal Area Networks (WPANs). http://grouper. ieee.org/groups/802/15/pub/2002/Nov02/02490r0P802-15_SG3a-Channel-Modeling-Subcommittee- Report-Final.zip.

[3] Part 15.4: Wireless Medium Access Control (MAC) and Physical Layer (PHY) Specifications for Low-Rate Wireless Personal Area Networks (WPANs) Amendment 1: Add Alternate PHYs.

[4] http://standards.ieee.org/getieee802/download/802. 15.4a-2007.pdf.

[5] Final / IEEE P802.15.4a Working Group for Wireless Personal Area Networks (WPANs), Dec. Channel Modeling *Sub-committee Report 2004.* http://grouper.ieee.org/groups/802/15/pub/04/15-04-0662-02-004a-channelmodel-final-report-r1.pdf.

[6] *Group for Wireless Personal Area Networks (WPANs).Channel Model for Body Area Network (BAN).* https://mentor.ieee.org/802.15/dcn/08/15-08-0780-12-0006-tg6-channelmodel.pdf.

International Innovative Research Journal of Engineering and Technology
ISSN: 2456-1983 Vol: 5 Issue: 2 December 2019

[7] F. Ramirez-Mireles, M. Z. Win, and R. A. Sholtz, in *Proc. 47th IEEE Vehicular Technology Conf., Phoenix, May 4–7, 1997* (IEEE, New York, 1997), Vol. 3, p. 2243.

[8] C. W. Kim, X. Sun, L. C. Chiam, et al., in *Proc. IEEE 2005 Wireless Communications and Networking Conf.,New Orleans, Mar. 13–17, 2005* (IEEE, New York, 2005), p. 950.

[9] UWB Channel Soundings and Models — Literature Overview. http://www.ieee802.org/15/pub/04/15-04-0196-00-004a-802-15-4a-channel-sounding-Overview.pdf.

[10] T. Santos, J. Karedal, P. Almers, et al., IEEE Trans. Wireless Commun. 9, 282 (2010).

[11] M. Di Renzo, F. Graziosi, R. Minutolo, et al., Mobile Networks Appl. 11, 451 (2006).

[12] H. Chaibi, M. Belkasmi, and Z. Mohammadi, in *Proc.2015 Int. Conf. Wireless Networks and Mobile Communications (WINCOM), Marrakech, Oct. 20–23, 2015* (IEEE, New York, 2015), p. 7381298.

[13] P. Richardson, W. Xiang, and D. Shan, Int. J. Ultra Wideband Commun. & Systems 3 (1), 060968 (2014).

[14] W. Khawaja, I. Guvenc, and D. Matolak, in *Proc. 2016 IEEE Global Communications Conf. (GLOBECOM),Washinghton, Dec. 4–8, 2016* (IEEE, New York, 2016), p. 7842372.

[15] Yu. V. Andreyev, A. S. Dmitriev, E. V. Efremova, et al., Int. J. Bifurcation & Chaos 15, 3639 (2005).

[16] M. G. Popov, Zh. Radioelektron., No. 6 (2014). http://jre.cplire.ru/jre/jun14/10/text.pdf.

[17] L. V. Kuz'min, J. Commun. Technol. Electron. 56, 367 (2011).

[18] B. Sklar, *Digital Communications. Fundamentals and Applications* (Prentice Hall PTR, Upper Saddle River, N. J., 2001; Vil'yams, Moscow, 2003).

[19] A. S. Dmitriev, E. V. Efremova, and M. Yu. Gerasimov, J. Commun. Technol. Electron. 60, 393 (2015).

[20] L. V. Kuz'min, A. I. Ryzhov, Yu. V. Andreev, and M. G. Popov, Fiz. Osnovy Priborostr. 7 (1/27), 91 (2018).

[21] L. V. Kuz'min and V. A. Morozov, J. Commun. Technol. Electron. 54, 313 (2009).

[22] L. V. Kuzmin, V. A. Morozov, S. O. Starkov, and B. A. Khadzhi, J. Commun. Technol. Electron. 51, 1283 (2006).

[23] S. Sharma, A. Gupta, and V. Bhatia, in *Proc. 2017 IEEE 85th Vehicular Technol. Conf. (VTC Spring), Sydney, June 4–7, 2017* (IEEE, New York, 2017).

[24] A. Maali, A. Mesloub, M. Djeddou, et al., IEEE Commun. Lett. 13, 959 (2009).

[25] M. Mroue, S. Haese, S. Paquelet, et al., in *Proc. 2007 IEEE Int. Workshop on Radio-Frequency Integration Technol., Singapore, Dec. 9–11, 2007* (IEEE, New York, 2007), p. 13.

[26] R. Vauche, E. Muhr, O. Fourquin, et al., IEEE Trans. Circuits Syst., I: Fundam. Theory Appl. 64, 1612 (2017).

[27] H. Chougrani, J. Schwoerer, P. H. Horrein, and A. Baghdadi, in *Proc. 2014 IEEE Int. Conf. on Ultra-WideBand (ICUWB), Paris, Sep. 1–3, 2014* (IEEE, New York, 2014).

[28] A. Mesloub, A. Boukhelifa, O. Merad, et al., IEEE Commun. Lett. 21, 2166 (2017).

[29] C. Gimeno, D. Flandre, and D. Bol, IEEE Trans. Circuits Syst., I: Fundam. Theory Appl. 65, 2015 (2018).

[30] Sai Sri, V. Harsha, and G. V. Mahalakshmi, in *Proc. 2016 Int. Conf. on Micro-Electronics and Telecommunication Engineering (ICMETE), Ghaziabad, Sep. 22–23,2016* (IEEE, New York, 2016).

[31] M. Daoud, H. Mnif, M. Ghorbel, and M. Loulou, in *Proc. IEEE 59th Int. Midwest Symp. on Circuits and Systems (MWSCAS), Abu Dhabi, 16–19 Oct. 2016* (IEEE, New York, 2016).

[32] S. Josephine, S. Chouhan, and A. Mahanta, in *Proc. 8th Int. Conf. on Commun. Systems and Networks (COMSNETS), Bangalore, Jan. 5–10, 2016* (IEEE, New York, 2016).

[33] E. V. Efremova, Usp. Sovremen. Radioelektron., No. 1, 17 (2008).

[34] A. Dmitriev, E. Efremova, L. Kuzmin, and N. Atanov, Int. J. Bifurcation and Chaos 17, 3443 (2007).

[35] *Analog Devices, "Data Sheet 1 MHz to 4 GHz, 80 dB, Logarithmic Detector Controller".* http://www.analog.com/media/en/technical-documentation/datasheets/ADL5513.pdf.

[36] Yu. V. Andreev, L. V. Kuz'min, V. A. Morozov, and S. O. Starkov, Usp. Sovremen. Radioelektron., No. 1, 63 (2008).

[37] Yu. V. Andreev, A. S. Dmitrieva, V. A. Lazarev, and A. I. Ryzhova, Usp. Sovremen. Radioelektron. No. 3, 55 (2013).

[38] Yu. V. Andreev, A. S. Dmitriev, V. A. Lazarev, and A. I. Ryzhov, in *Proc. Sci. Conf. "III All-Russian Armandovsky Readings", Murom, Iune 26–28, 2013* (MIVlGU, Vladimir, 2013), p. 75.